Temperature evolution of topological surface states in Bi_2Se_3 thin films studied using terahertz spectroscopy

Varun S. Kamboj*[a], Angadjit Singh[a], Harvey E. Beere[a], Thorsten Hesjedal[b], C.H.W Barnes[a] and David A. Ritchie[a]

[a]Cavendish Laboratory, University of Cambridge, J. J. Thomson Avenue, Cambridge CB3 0HE, United Kingdom;
[b]Department of Physics, Clarendon Laboratory, University of Oxford, Oxford OX1 3PU, United Kingdom;

ABSTRACT

We have measured the terahertz (THz) conductance of a 23 quintuple layer thick film of bismuth selenide (Bi_2Se) and found signatures for topological surface states (TSSs) below 50 K. We provide evidence for a topological phase transition as a function of lattice temperature by optical means. In this work, we used THz time-domain spectroscopy (THz-TDS) to measure the optical conductance of Bi_2Se_3, revealing metallic behavior at temperatures below 50 K. We measure the THz conductance of Bi_2Se_3 as 10 e^2/h at 4 K, indicative of a surface dominated response. Furthermore, the THz conductance spectra reveal characteristic features at ~1.9 THz attributed to the acoustic phonon mode, which is weakly visible at low temperatures but which becomes more prominent with increasing temperature. These results present a first look at the temperature-dependent behavior of TSSs in Bi_2Se_3 and the capability to selectively identify and address them using THz spectroscopy.
Keywords: terahertz, topological insulators, spectroscopy, bismuth selenide.

1. INTRODUCTION

Topological insulators (TIs) present a new state of quantum matter with insulating bulk and robust conducting surface states. These topological surface states (TSSs) are protected by the time reversal symmetry and strong spin orbit interaction[1-4]. TSSs of a 3D TI consist of an odd number of Dirac cones in the surface Brillouin zone, guaranteed by the Z_2 topological invariant of the bulk[4,5]. In the simplest scenario with a single Dirac cone, such as on the surface of Bi_2Se_3,[6-9] the surface states can be described by Rashba spin orbit coupling[10] and show a helical behavior[11]. These metallic surface states have been proposed to have a wide range of applications from spintronics[1,7,12] to quantum computing[13]. In an ideal TI the bulk does not contribute to charge transport and the conductivity is solely a result of surface carriers. However, the present generation of TIs, particularly Bi_2Se_3 exhibits significant contributions from the bulk carriers to the net conductance. The primary reason for such a behavior is shifting of the electrochemical potential into the conduction band due to selenium (Se) vacancies and anti-site defects[14]. Moreover, if the Fermi level crosses the bulk band near the surface, it can lead to the formation of a two-dimensional electron gas (2DEG) due to bending of the bands near the surface. Such a 2DEG is limited to within ~20 nm of the surface[15,16] and occurs alongside the TSSs.

The functionality of TIs as a viable material for novel applications in technology requires unambiguous separation of the surface state response from the interfering bulk and quantum well states (QWSs). Conventional transport measurements suffer a drawback due to simultaneous measurement of TSSs and the bulk carriers, in both thin film and single crystal TIs. The TSSs differ from the bulk states and QWSs in their topological origin. Although angle-resolved photoemission spectroscopy (ARPES) can probe the TSSs directly, its sensitivity is limited to the surface carriers, lacking the high energy resolution near the electrochemical potential[17]. It would be highly desirable to have a technique which can detect and isolate the TSSs from the bulk contribution unambiguously with the capability to selectively address the TSSs for real world applications. Terahertz (THz) spectroscopy is an optical technique, free of contacts to probe the low-energy

*E-mail: vk302@cam.ac.uk , Phone: +44 1223 768142

excitations in strongly correlated electron gases. It has been recently reported that THz-TDS can be used identify TSSs contributions in $Bi_{1.5}Sb_{0.5}Te_{1.8}Se_{1.2}$ (BSTS), but identifying surface from the bulk was not possible, due to defects and surface deterioration[18]. A temperature dependent THz study which would unambiguously demonstrate a transition from bulk response to TSSs would be highly desirable, for practical applications. Here, we report the use of broadband THz-TDS to identify TSSs from the bulk and QWSs by measuring the THz transmittance of Bi_2Se_3 thin film as a function of temperature. We demonstrate a transition from a bulk like response dominant at high temperatures, to a TSSs metallic response at low temperatures with the transition around 50 K and therefore present a non-destructive method to selectively identify and address the TSSs in Bi_2Se_3.

2. MBE THIN-FILM GROWTH

Molecular beam epitaxy (MBE) was used to grow 23 QLs (1 QL = 0.954 nm) of Bi_2Se_3 on a c-plane sapphire (0001) substrate, in a UHV system with a base pressure of $1x10^{-10}$ torr. Standard effusion cells were used to evaporate pure elemental source materials (Bi (6N) and Se (6N)). The film was synthesized in two stages: first a 5.8-nm-thick Bi_2Se_3 seed layer was grown at a substrate temperature of 250°C, followed by an annealing step with the substrate temperature raised to 300°C. This process reduces the twinning effect[19], commonly observed in this materials system. The corresponding flux ratio for Bi: Se was 1:10, as recorded by a beam flux monitor. The final 16.2-nm-thick Bi_2Se_3 layer was grown keeping the substrate at 300°C. X-ray diffraction (XRD) was performed (cf. Fig. 1 a), which shows peaks of the (00l) family of Bi_2Se_3, confirming the high crystalline quality.

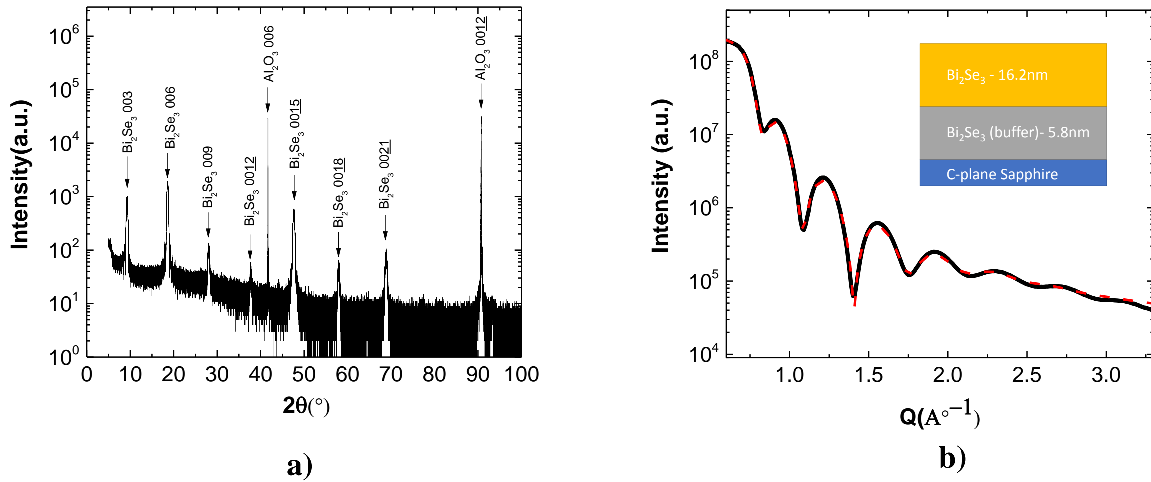

Figure 1: a) Out-of-plane 2θ-ω XRD scan for the 23-QL-thick (22 nm) Bi_2Se_3 film with major peaks identified as incidated. θ denotes the angle between the x-ray beam and the plane of the sample. b) X-ray reflectivity (XRR) plot for the Bi_2Se_3 film. The black and the red lines represent the raw data and the fit, respectively.

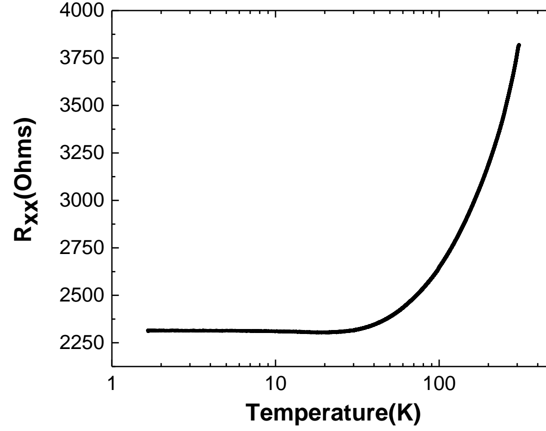

Figure 2: Temperature-dependent longitudinal resistance for the 23-QL-thick Bi_2Se_3 film.

The x-ray reflectivity (XRR) plot is shown in Fig. 1 b). The modelling was done by considering two layers of Bi_2Se_3 with the density varying at the substrate interface to enable proximity effects (inset of Fig.1 b). The model shows a total Bi_2Se_3 layer thickness of 22 nm, consisting of a 5.8-nm-thick seed layer and a 16.2-nm-thin film with a surface roughness of 1.7 nm. Electrical transport measurements wer carried out in a continuous flow He cryostat with a base temperature of 1.7 K at 33 Hz. Our samples were processed into Hall bars using photolithography as reported previously[20]. Figure 2 shows the temperature-dependent longitudinal resistance (R_{xx}). In the range from room temperature to 50 K, the resistance shows a monotonic decrease which is attributed to electron-phonon scattering[21]. The is confirmed by the reducing phonon peak at 1.9 THz in this temperature range, as seen in the real part of the conductance spectra (Fig. 4a), discussed in further detail below. However, close to 50 K, the resistance levels out indicating the freezing out of the bulk carriers. The region below 50 K is likely to be dominated by surface conduction and impurity states (QWSs), which is in good agreement with previous reported results[27] for similar thicknesses.

3. TERAHERTZ CONDUCTIVITY

Broadband terahertz time domain spectroscopy (TDS) was carried out on the 23-QL-thick Bi_2Se_3 film, grown by MBE. The sample was mounted in the cryostat with optical access to obtain a temperature dependent THz response. The measurements were carried out with a Tera K15- T-Light MENLO system, with a 60 mW pump pulse focused down to a 40 μm spot onto the THz emitter, resulting in a broadband THz emission with a spot size of ~1 mm. To probe the temperature-dependent optical conductivity of Bi_2Se_3, we measured the complex optical conductance $\tilde{G}(\omega) = G_1(\omega) + iG_2(\omega)$ of the TI film and extracted the real and imaginary part of conductance as a function of frequency ω. It should be noted that the real and imaginary conductance have been measured concurrently, however, they are independent of each other. The imaginary conductance is associated with the phase shift with respect to the reference substrate, and hence can be used to deduce mobility and scattering rate of carriers in the TI film. This makes THz-TDS a powerful tool to measure key material parameters related to TI thin films. Analysis of the low frequency limit THz conductance can be used to examine the quasi d.c transport properties, in a non-contact and non-destructive manner.

Figure 2 a) shows the time-resolved THz transmission through the Bi_2Se_3 thin film at different temperatures. The THz field for the Bi_2Se_3 shows a time delay and reduced amplitude relative to the signal through air, reflecting both the thickness and refractive index of the sample. Figure 2 b) shows a magnified view of the THz field at various lattice temperatures. We observe that the transmitted THz field intensity increases with reducing temperature down to 50 K, after which it decreases with further reduction in temperature to 4 K. The power transmission spectra demonstrating absorption from the free-carriers in the Bi_2Se_3 film, shedding further light on this behavior.

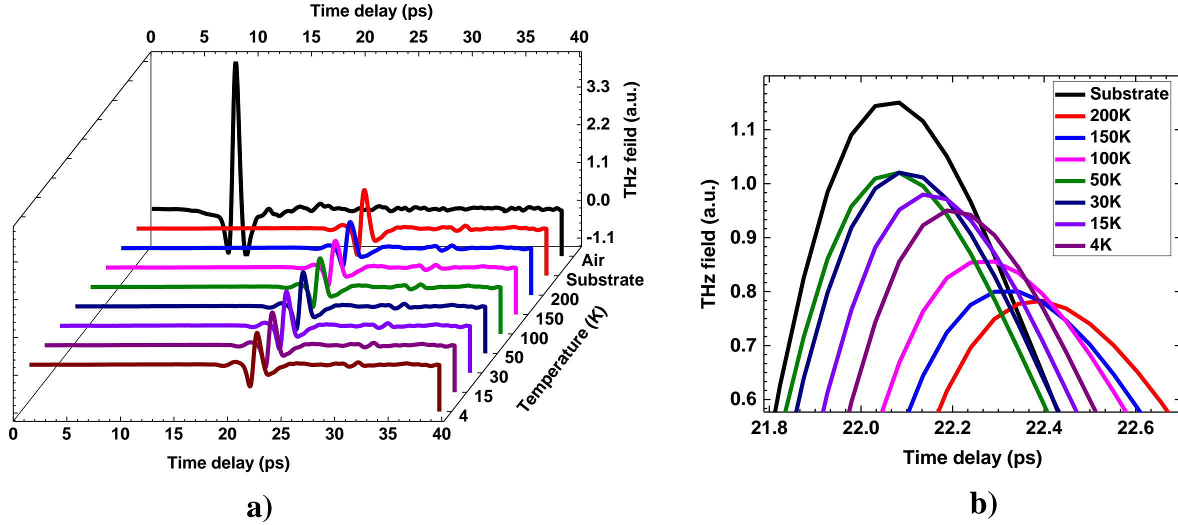

Figure 2: a) Time domain picosecond (ps) pulse response transmitted through air and a Bi_2Se_3 film (60 nm) at different temperatures. b) Magnified pulse response transmitted through the Bi_2Se_3 film. The substrate is sapphire (0001).

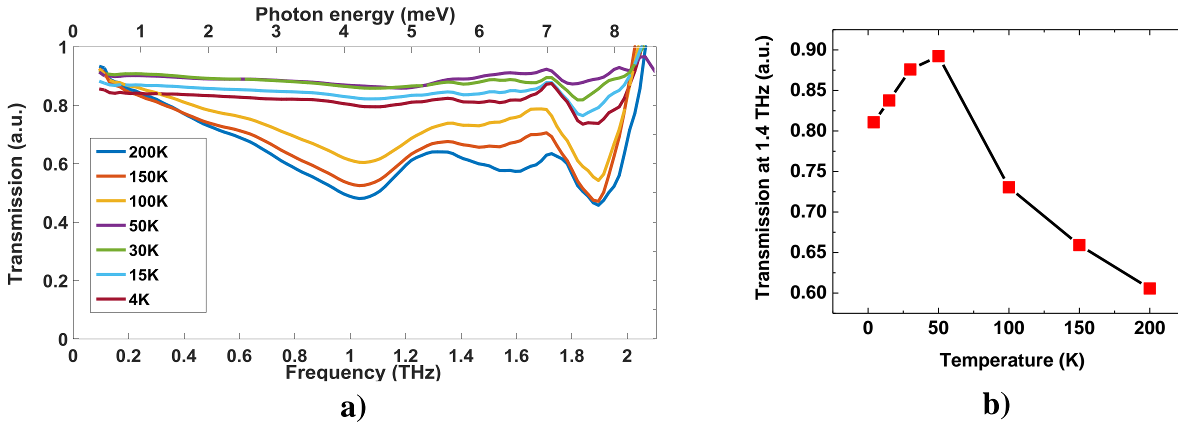

Figure 3: a) Power transmission spectra calculated from the Fourier transform of the primary transmitted peak through Bi_2Se_3 and normalized to the transmission through the sapphire (0001) substrate for each temperature. b) The transmission first increases and then decreases with falling temperature, indicating the presence of two different topological phases at low and high temperatures.

The power transmission spectra, *T*, shown in Fig. 3a), were calculated from the Fourier transform of the primary transmitted peak through Bi_2Se_3 and normalized to the transmission through the sapphire substrate for each temperature. We observe that *T* increases with decreasing temperature down to 50 K, exhibiting free carrier absorption. However, below 50 K the transmission falls as the lattice temperature is reduced to 4 K. The transmission (at 1.4 THz) as a function of temperature shown in Fig. 3 b) explains the initial upsurge in the time domain response (Fig. 2 b). Such behavior is indicative of the presence of two different phases in Bi_2Se_3 with different properties and distinct spectral features. The power transmission also shows a broad dip around 1 THz (4.1 meV), which corresponds to the intersubband transitions in the QWSs. The QWSs form a 2DEG confined to the surface, which is equivalent to a one-dimensional quantum well system and appear as distinct features in the power transmission spectra. The presence of the QWSs in thin film Bi_2Se_3 has been confirmed by ARPES measurements previously[22,23]. The QWSs formed from the band bending (or from Se vacancies) near the surface can be described with a triangular potential well model, as discussed in a previous report[24], allowing us to assign the absorption peak at 1.0 THz to the so-called intersubband-band transition. The power transmission spectra also show a strong dip at 1.9 THz (8 meV) depicting the optical phonon mode (α-phonon). The spectral features observed in the transmission spectra are in good agreement with previous studies on Bi_2Se_3,[25,26]. Furthermore, both the features in the

transmission spectra show strong temperature-dependent behavior with a systematic transition from bulk-like behavior to a surface response as elucidated by obtaining the THz conductance.

We further calculated the optical conductance using Tinkham's theory[27] to obtain the spectral response as presented in Fig. 4 a). Since the THz-TDS measures both the amplitude and phase of the signal, there is no need to employ the Kramers-Kronig transformation to obtain the real and imaginary components of the optical parameters. The conductance $G(\omega)$ of a TI film of thickness *t* can be described according to the Drude-Lorentz relationship,

$$G(\omega) = \frac{i\omega_{TSS}}{4\pi\,(\omega + i\gamma_{TSS})} + \frac{i\omega_{QWS}}{4\pi\,(\omega + i\gamma_{QWS})} - \frac{i\omega t}{4\pi}\frac{S_{QWS}^2}{\left(\omega^2{}_{0,QWS} - \omega^2 - i\Gamma_{QWS}\,\omega\right)} \quad (1)$$

where ω_{TSS} (ω_{QWS}) and γ_{TSS} (γ_{QWS}) denote the plasma frequency and the scattering rate, respectively, for the TSSs (QWSs), while S_{QWS}, $\omega_{0,QWS}$ and Γ_{QWS} represent the oscillator strength, center frequency, and the damping rate of intersubband transitions in the QWSs[25], respectively. The THz conductance (Fig. 4a) shows an overall decline as the temperature falls to 50 K, implying the freezing of bulk charge carries in Bi_2Se_3. We identify the broad signatures at 1 THz and the sharp peak at 1.9 THz as the contributions from the QWSs and the optical phonon, respectively, as discussed earlier. Imaginary conductivity spectra (Fig. 4b) show the accompanying phase distortions in the real part of the conductance. The diminishing QWSs response has been observed previously[24] with reducing film thickness. As the temperature decreases from 200 K to 4 K we expect a reduced contribution from the bulk and QWSs, thus leaving the TSSs (the top and bottom) as the main contributor to the measured conductance values.

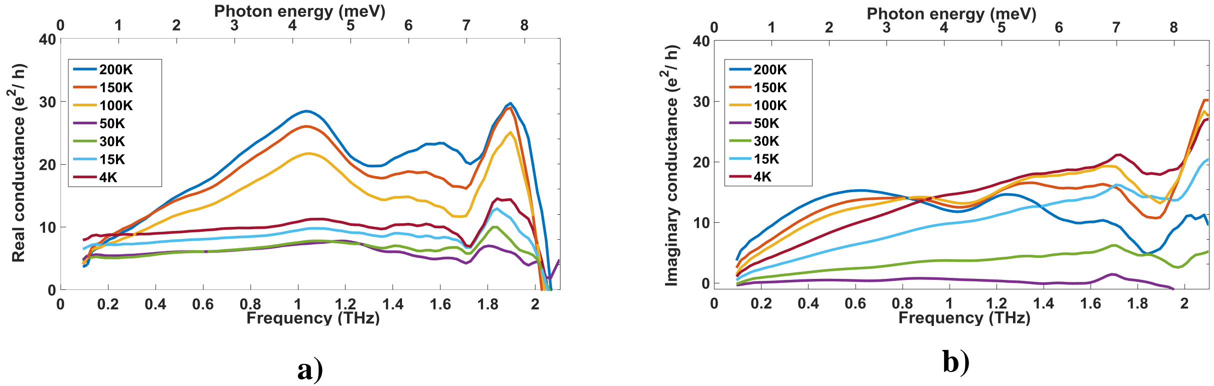

Figure 4: a) Real conductance spectra showing distinct features at around 1.0 THz, referring to intersubband transitions in QWSs, and 1.9 THz, referring to the optical phonon mode (α-phonon). b) Imaginary conductance spectra reflecting the accompanying phase distortions in the real conductance.

The THz conductance spectra confirm the emergence of TSS phenomena in Bi_2Se_3 below 50 K. The real conductance value at 1.4 THz increases from ~7 e^2/h to 10 e^2/h, as the lattice temperature is reduced from 50 K to 4 K, confirming the advent of a metal-like surface behavior, characteristic of TSSs (Fig.5 a). It is interesting to note that our transport measurements (Fig. 2) reveal a change in the longitudinal resistance at 50 K, providing further evidence for surface-dominated response below 50 K.

The low frequency extrapolation of the real conductance spectra should approach the d.c. conductance values obtained from standard transport measurements. It should be noted that transport measurements rely heavily on the device processing and geometry making it difficult to obtain a TSSs response from pristine surface of a TI. Bansal *et al.*[28] have discussed the difficulty in distinguishing the TSS contribution from the noisy background, particularly for ultra-thin films. The THz conductance measurement present an alternative way of obtaining the quasi-d.c. value of conductance in TIs. The metallic behavior of THz conductance at low temperatures is fairly uniform across the entire frequency range (0.1-2.2 THz). It should be noted that our measurement stands out as a technique to probe both the surface and bulk states; the frequency dependent conductance $\tilde{G}(\omega)$ can demonstrate a more surface sensitive response at higher frequencies, limited by the bandwidth of the THz photoconductive detector, due to the skin depth effect.

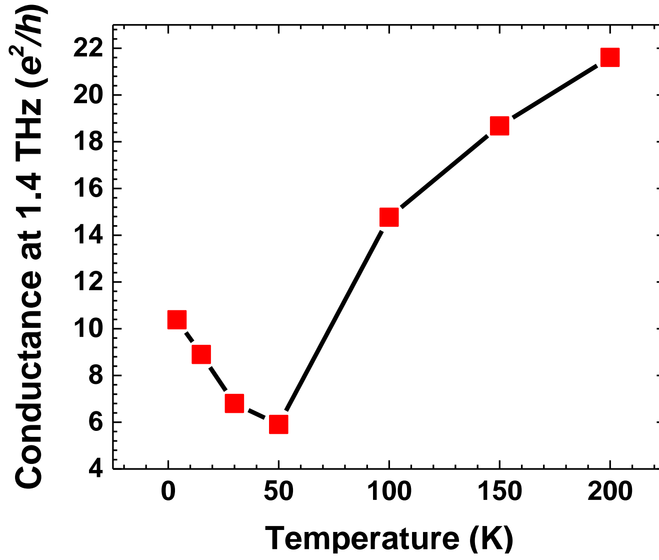

Figure 5: Real part of the conductance at 1.4 THz as function of temperature showing metallic behavior below 50 K.

The skin depth δ dependence on the frequency f is given by the equation $\delta = \sqrt{\rho/(\pi f \mu_0 \mu_r)}$, where ρ is the resistivity and μ_r is the relative permeability of the film. At higher frequencies approaching 2.2 THz, the skin depth of the THz field would be relatively smaller, thus measuring a response much closer to the surface of the TI.

Our transport measurements (Fig. 2) show the longitudinal resistance at 4 K to be 2.3 kΩ (11.2 e^2/h), in close agreement with our THz optical conductance value of 10 e^2/h at 4 K. The transport measurement, calculating the surface conduction in Bi_2Se_3 previously reported[29], are also in good agreement with our THz quasi-d.c. values of ~10 e^2/h, in the surface-dominated regime at 4 K. It is worth mentioning that we rule out QWSs contribution from the low temperature metallic behavior of the THz conductance, since our THz conductance spectra clearly shows a diminishing response at ~1 THz, which was attributed to QWSs. To further establish the distinct signature of TSSs from 2DEG at low temperature, requires the measurement of temperature-dependent carrier concentration (sheet carrier density). The sheet carrier density for a TI and a 2DEG is given as $n_{SC(TI)} = {k_{F,TI}}^2/(4\pi)$ and $n_{SC(2DEG)} = {k_{F,2DEG}}^2/(2\pi)$, where k stands for the Fermi-wave vector[28]. Since the fermi-wave vector for TSSs is larger than for the 2DEG, we should always have $n_{SC(TI)} > n_{SC(2DEG)}$. This can be established through a THz optical conductance measurement with gated-field effect transistor type device[30], where a gate can tune the Fermi level across the bandgap, to obtain a TSS selective response.

4. CONCLUSION

THz spectroscopy provides a novel technique to confirm the presence of TSSs in quantum materials and explore the rich physics at low temperature in TIs. We have demonstrated that THz-TDS can be used to unambiguously detect the TSSs in Bi_2Se_3 at temperatures below 50 K. The conductance spectra show clear features of QWSs which flattens out with reducing temperature. Moreover, we observe clear signatures of a metallic behavior characteristic of the TSSs, in the low temperature regime below 50 K. Our transport measurements exhibited a similar transition temperature of 50 K, signifying the onset of a surface state behavior. The direct coupling between the TSSs and optical radiation in the sub-THz frequency range, opens up the possibly of developing novel TI devices such as modulators and detectors[31], operating in the THz gap. Therefore, the THz-TDS implemented in this work will open up the possibility of studying and developing future quantum TI devices for practical applications.

5. ACKNOWLEDGMENTS

The authors of this manuscript acknowledge financial support from the Engineering and Physical Sciences Research Council (EPSRC), grant numbers EP/J017671/1 - Coherent Terahertz Systems (COTS).

REFERENCES

1. M. Z. Hasan & C.L. Kane, *Rev. Mod. Phys.* **82**, 3045–3067 (2011).
2. X. L. Qi & S. C. Zhang, *Rev. Mod. Phys.* **83,** PAGES (2011).
3. M. Z. Hasan and J. E Moore, *Annu. Rev. Condens. Matter Phys*. **2**, 55-?? (2011).
4. L. Fu, C. L. Kane, E. J. Mele, *Phys. Rev. Lett.* **98,** 1–4 (2007).
5. J. E. Moore, L. Balents, *Phys. Rev. B* **75,** 3–6 (2007).
6. H. J. Zhang, C. X. Liu, X. L. Qi, X. Dai, Z. Fang, and S.C. Zhang, *Nat. Phys*. **5**, 438-??? (2009).
7. Y. Xia, D. Qian, D. Hsieh, L. Wray, A. Pal, H. Lin, A. Bansil, D. Grauer, R. J. Cava, and M. Z. Hasan, *Nat. Phys.* **5**, 398-??? (2009).
8. Y. L. Chen, J. G. Analytis, J. H. Chu, Z. K. Liu, S. K. Mo, X. L. Qi, H. J. Zhang, D. H. Lu, X. Dai, Z. Fang, S. C. Zhang, I. R. Fisher, Z. Hussain, and Z. X. Shen, *Science* **325**, 178-??? (2009).
9. D. Hsieh, Y. Xia, D. Qian, L. Wray, F. Meier, J. H. Dil, J. Osterwalder, L. Patthey, A. V. Fedorov, H. Lin, A. Bansil, D. Grauer, Y. S. Hor, R. J. Cava, and M. Z. Hasan, *Phys. Rev. Lett.* **103**, 146401 (2009).
10. Y. A. Bychkov and E. I. Rashba, *J. Phys. C* **17**, 6039-???? (1984).
11. C. X. Liu, X. L. Qi, H. J. Zhang, X. Dai, Z. Fang, and S.C. Zhang, *Phys. Rev. B* **82**, 045122 (2010).
12. L. Fu and C. L. Kane, *Phys. Rev. Lett.* **100**, 096407 (2008)
13. D. Hsieh, D. Qian, L. Wray, Y. Xia, Y. S. Hor, R. J. Cava & M. Z. Hasan, *Nature* **452**, 970–974 (2008).
14. M. Brahlek, Y. S. Kim, N. Bansal, E. Edrey, and S. Oh, *Appl. Phys. Lett.* **99**, 012109 (2011).
15. M. Bianchi, D. Guan, S. Bao, J. Mi, B. Iversen, P. King, and P. Hofmann, *Nat. Commun.* **1**, 128 (2010).
16. P. D. C. King, R. C. Hatch, M. Bianchi, R. Ovsyannikov, C. Lupulescu, G. Landolt, B. Slomski, J. H. Dil, D. Guan, J. L. Mi, E. D. L. Rienks, J. Fink, A. Lindblad, S. Svensson, S. Bao, G. Balakrishnan, B. B. Iversen, J. Osterwalder, W. Eberhardt, F. Baumberger, and P. Hofmann, *Phys. Rev. Lett.* **107**, 096802 (2011).
17. R. Valdés Aguilar, J. Qi, M. Brahlek, N. Bansal, A. Azad, J. Bowlan, S. Oh, A. J. Taylor, R. P. Prasankumar, and D. A. Yarotski, *Appl. Phys.Lett*. **106**, 011910 (2015).
18. C. S. Tang, B. Xia, X. Zou, S. Chen, H.-W. Ou, L. Wang, a Rusydi, J.-X. Zhu, and E. E. M. Chia, *Sci. Rep*. **3**, 3513 (2013).
19. S. E. Harrison, S. Li, Y. Huo, B. Zhou, Y. L. Chen, and J. S. Harris, *Appl. Phys. Lett.* **102**, 171906 (2013).
20. L. J. Collins-McIntyre, L. B. Duffy, A. Singh, N.-J. Steinke, C. J. Kinane, T. R. Charlton, A. Pushp, A. J. Kellock, S. S. P. Parkin, S. N. Holmes, C. H. W. Barnes, G. van der Laan, S. Langridge, and T. Hesjedal, *Europhys. Lett.* **115,** 27006 (2016).
21. D. Kong, Y. Chen, J. J. Cha, Q. Zhang, J. G. Analytis, K. Lai, Z. Liu, S. S. Hong, K. J. Koski, S. K. Mo, Z. Hussain, I. R. Fisher, Z. X. Shen, and Y. Cui. *Nat. Nanotechnol.* **6,** 705–709 (2011).
22. A. Richardella, D. M. Zhang, J. S. Lee, A. Koser, D. W. Rench, A. L. Yeats, B. B. Buckley, D. D. Awschalom, and N. Samarth. *Appl. Phys. Lett.* **97**, 262104 (2010).
23. E. Wang, H. Ding, A. V. Fedorov, W. Yao, Z. Li, Y.-F. Lv, K. Zhao, L.-G. Zhang, Z. Xu, J. Schneeloch, R. Zhong, S. H. Ji, L. Wang, K. He, X. Ma, G. Gu, H. Yao, Q. K. Xue, X. Chen, and S. Zhou, *Nat. Phys.* **9,** 621–625 (2013).
24. H. M. Benia, C. Lin, K. Kern, and C. R. Ast, *Phys. Rev. Lett.* **107,** ARTICLE-# (2011).
25. B. C. Park, T. H. Kim, K. I. Sim, B. Kang, J. W. Kim, B. Cho, K. H. Jeong, M. Cho and J. H. Kim. *Nat. Commun.* **6,** 6552 (2015).
26. R. Valds Aguilar, A. V. Stier, W. Liu, L. S. Bilbro, D. K. George, N. Bansal, L. Wu, J. Cerne, A. G. Markelz, S. Oh, and N. P. Armitage. *Phys. Rev. Lett.* **108,** ARTICLE-# (2012).
27. Martin C. Nuss and Joseph Orenstein. *Millimeter and Submillimeter Wave Spectroscopy of Solids*. Springer-Verlag Berlin Heidelberg, 1998.
28. N. Bansal, Y. S. Kim, M. Brahlek, E. Edrey, and S. Oh, *Phys. Rev. Lett.* **109**, 116804 (2012).
29. N. Koirala, M. Brahlek, M. Salehi, L. Wu, J. Dai, J. Waugh, T. Nummy, M. G. Han, J. Moon, Y. Zhu, D. Dessau, W. Wu, N. P. Armitage, and S. Oh, *Nano Lett.* **15,** 8245–8249 (2015).

30. D. Kim, S. Cho, N. P. Butch, P. Syers, K. Kirshenbaum, S. Adam, J. Paglione, M. S. Fuhrer, *Nat. Phys.* **8,** 459–463 (2012).
31. L. Viti, D. Coquillat, A. Politano, K. A. Kokh, Z. S. Aliev, M. B. Babanly, O. E. Tereshchenko, W. Knap, E. V. Chulkov, and M. S. Vitiello, *Nano Lett.* **16,** 80–87 (2016).